Effect of porcine reproductive and respiratory syndrome virus 2 on angiogenesis and cell proliferation at the maternal-fetal interface

Veterinary Pathology
2022, Vol. 59(6) 940–949

DOI: 10.1177/0300985822105053
journals.sagepub.com/home/vet


Javier A. Barrera-Zarate[1], Susan E. Detmer[1], J. Alex Pasternak[2], Glenn Hamonic[1], Daniel J. MacPhee[1], and John C. S. Harding[1]

Abstract

Angiogenesis and cell proliferation in reproductive tissues are essential events for the maintenance of pregnancy, and alterations can lead to compromised fetal development and survival. Porcine reproductive and respiratory syndrome virus 2 (PRRSV-2) induces reproductive disease with negative financial and production impact on the swine industry. PRRSV-2 infection alters placental physiology through inflammatory and apoptotic pathways, yet fetal susceptibility varies. This study aimed to evaluate angiogenesis and cell proliferation in the porcine maternal-fetal interface (MFI) and determine if these physiological processes were altered by PRRSV-2 infection. Thirty-one pregnant gilts were inoculated with PRRSV-2 at gestation day 86 ± 0.4 (mean ± SD). Seven control gilts were sham-inoculated. All gilts were euthanized at 12 days postinoculation. Angiogenesis and cell proliferation were determined through the detection of vascular endothelial growth factor (VEGF) and Ki-67, respectively, using immunofluorescence of the MFI from 4 fetal resilience groups: uninfected (UNIF), high viral load–viable (HVL-VIA), and HVL-meconium-stained (MEC) from PRRSV-infected gilts, as well from sham-inoculated (CON) gilts. VEGF immunolabeling in the uterine submucosa was significantly lower in MEC compared with UNIF and HVL-VIA groups. Significantly greater Ki67 immunolabeling was detected in the trophoblasts of CON fetuses versus all other groups, and in uterine epithelium of CON and UNIF fetuses versus HVL-VIA and MEC. These results suggest that fetal resilience may be related to greater cell proliferation in uterine epithelium, and fetal compromise with reduced uterine submucosal angiogenesis, except fetuses with intrauterine growth restriction, in which inherently lower submucosal angiogenesis may be protective against PRRSV infection.

Keywords

angiogenesis, PRRSV, maternal-fetal interface, fetomaternal junction, swine, fetus, disease resilience, intrauterine growth restriction

Porcine reproductive and respiratory syndrome virus 2 (PRRSV-2) (*Betaarterivirus suid 2*) causes disease characterized by reproductive failure and interstitial pneumonia in growing pigs and is considered one of the most significant viral pathogens in pig production due to economic and production losses in breeding and feeding herds.[17,29,44] Reproductive losses are primarily due to late-term abortions and fetal death, but also include birth of stillborn and weak congenitally infected piglets, as well as infertility.[22,27,43] The growing pig losses are primarily associated with the role that PRRSV-2 plays in the porcine respiratory disease complex that leads to increased nursery mortality and morbidity.[29] Moreover, PRRSV-2 is a profoundly immunosuppressive virus, exerting effects on both the innate and adaptive responses.[24]

Despite the severe reproductive disease caused by many PRRSV-2 strains, the cellular mechanisms used by the virus to compromise fetal survival during the last third of gestation have not been determined. Within days of maternal infection, the virus may cross the maternal-fetal interface (MFI; that is, the adherent uterine and fetal chorioallantois-allantochorion) to infect fetuses by way of the umbilical circulation,[26,42] but the timing of infection varies among fetuses within a litter, and some fetuses escape infection. Different phenotypic fetal categories related to preservation states and viral load have been established to investigate factors associated with fetal resilience. Fetal preservation is based on the viability and gross lesions of the fetus at the time of necropsy and classified as viable, meconium-stained (MEC), decomposed (recent death), and autolyzed (early death).[22,26] PRRSV RNA concentration in fetal thymus, serum, and placenta varies between states of fetal preservation.[22] Fetuses may be classified as high viral load

[1]University of Saskatchewan, Saskatoon, SK, Canada
[2]Purdue University, West Lafayette, IN

Supplemental material for this article is available online.

Corresponding Author:
Susan E. Detmer, Department of Veterinary Pathology, Western College of Veterinary Medicine, University of Saskatchewan, 52 Campus Drive, Saskatoon, SK S7N 5B4, Canada.
Email: susan.detmer@usask.ca

(HVL), low viral load (LVL), or uninfected (UNIF). UNIF are fetuses from infected dams where viral RNA is not detected in serum or thymus of the fetus, which are therefore considered relatively resistant compared with their HVL cohorts.

Fetal compromise is likely associated with PRRSV-related events occurring at the MFI, within the fetus or a combination of the two. While critical physiological changes in the fetus including hypothyroidism,[34] cytokine expression,[33,47] hypoxia and apoptosis,[25] and endocrine disruption are related to fetal compromise, the lesions in endometrium and placenta associated with PRRSV-2 infection may alter the normal transplacental nutritive and physiological processes essential for fetal growth and survival. The most consistent microscopic lesions in reproductive tissues associated with PRRSV-2 infection are inflammation and vasculitis in the endometrium[30,32] as well as apoptosis in placental endothelial cells, uterine epithelial cells (UECs), and trophoblasts[19,30,31] that historically have been considered important maternal factors contributing to reproductive failure.

The porcine fetomaternal junction (FMJ; including the interdigitating trophoblastic epithelium and uterine epithelium) continually remodels throughout pregnancy through processes of apoptosis, cell proliferation, and angiogenesis to maintain and support fetal development and survival.[39,41,46] Given the extensive lesions in the MFI following PRRSV infection and the wide variation in fetal outcome, it is possible that alterations in angiogenesis and cell proliferation at the MFI also contribute to fetal outcome. This study aimed to evaluate angiogenesis and cell proliferation in the porcine MFI following maternal PRRSV-2 infection and to determine whether alterations in these processes were associated with variation in fetal resilience.

Materials and Methods

Animal Experimental and Sample Collection

Thirty-one pregnant purebred Landrace gilts were intramuscularly and intranasally inoculated with PRRSV-2 (NVSL 97-7895 propagated on MARC-145 cells; 1×10^5 $TCID_{50}$ total dose) on gestation day 86 ± 0.4 (mean ± SD). At the same gestational stage, 7 pregnant control gilts (CON) were similarly sham-inoculated with sterile minimum essential media. All the gilts were euthanized by intravenous barbiturate overdose (Euthanyl Forte, 19,200 mg/gilt) and cranial captive bolt at 12 days postinfection. The study protocols have been described in detail,[25,34] adhered to guidelines established by the Canadian Council on Animal Care, and were reviewed and approved by the University of Saskatchewan Animal Research Ethics Board (permit #20160023).

At necropsy, the gravid uterus was removed and fetuses counted sequentially based on their position in each horn (starting with L1/R1 at the tip of the left and right horns, respectively). The external fetal preservation status was assessed as viable (VIA; live with normal skin color), MEC (live and MEC on head and/or body), or decomposed (DEC; dead with pale skin ± edema) as previously described.[22,30] Fetuses were subsequently weighed, sexed, and dissected. The weights of key organs including brain and liver were recorded and used to assess the proportionate growth of brain compared with liver as a proxy measure for intrauterine growth restriction (IUGR; high brain: liver weight ratio).[2,22]

Sampling of the MFI was performed by cutting the uterine wall (full thickness) into rectangular samples (approximately 3 × 20 cm^2). From the MFI associated with each fetus ($n = 516$), 3 samples were collected: centered on the umbilical stump (sample 1), 10 to 15 cm distant from the umbilical stump toward the ovary (sample 2), and 0 to 15 cm distant from the umbilical stump along the anti-mesometrial border (sample 3).[25] All samples were fixed in 10% buffered formalin, trimmed to 1-cm squares and processed routinely for hematoxylin and eosin staining. Histological analyses of these sections evaluating the severity of inflammation in the endometrium, placenta, and blood vessels was performed as previously described.[32] Briefly, the inflammation scores in the endometrium and placenta were categorized as, score 0 for no inflammatory cell infiltrate in the tissues; score 1 for less than 10% of tissue section with inflammatory cell infiltrate; score 2 for 10% to 25% of tissue section; score 3 for 25% to 50% of tissue section; and score 4 for greater than 50% of tissue section with inflammatory cell infiltrate. Scores for inflammation within the vascular walls (vasculitis) in the endometrium and placenta were classified as score 0 for no vasculitis; score 1 for vasculitis in less than 30% of blood vessels; score 2 for 30% to 70%; and score 3 for greater than 70% of inflamed blood vessels in the tissue sections.

Assessment of Fetal Viral Load

Fetal viral load was evaluated by RT-qPCR as previously described in detail.[22,25] Briefly, RNA was extracted from 140 µL of fetal sera using QIAamp Viral RNA mini kit and from 10 to 20 mg tissue (allantochorion and fetal thymus) using RNeasy extraction kit (Qiagen). A strain-specific probe-based protocol targeting open reading frame 7 (ORF7) with a 5-point standard curve (10^7, 10^5, 10^3, 10^2, 10^1) run in triplicate on each plate was used for quantification. Samples were run in duplicate in 96-well plates using corresponding positive controls. Viral concentration was reported as $\log_{10}$ target copies per mg/µL tissue/sera. The limits of quantification were defined by the least and most concentrated standards, the lower limit being 2.2 $\log_{10}$ per uL sera or mg tissue.

Fetal Classification

A classification system representative of disease progression[34] was used to select a subset of fetuses for further analysis. First, control fetuses were randomly selected from 7 CON gilts. From PRRSV-2-infected gilts, groups were selected as follows (Table 1): UNIF (live fetuses with nondetectable/negative PRRSV RT-qPCR [reverse transcriptase quantitative polymerase chain reaction] in fetal placenta, sera, and thymus), high viral load–viable (HVL-VIA: live fetus with >4.4 $\log_{10}$ genome copies per mg/µL in placenta, sera, and thymus), and

Table 1. Summary of median histologic lesion severity scores and PRRS viral load by fetal group.

	PRRS histological lesion scores (minimum/maximum)				PRRSV RNA concentration		
Group	Endometritis	Vasculitis endometrium	Placentitis	Vasculitis placenta	Placenta	Serum	Thymus
CON	0[a]	0[a]	0[a]	0	NA	NA	NA
(n = 12)	(0/0)	(0/0.3)	(0/0)	(0/0)			
UNIF	3.0[b]	2.6[b]	0[b]	0	0.0[a]	0.0[a]	0[a]
(n = 10)	(1.6/3.6)	(1/3)	(0/1.3)	(0/0)	(0/0)	(0/0)	(0/1.3)
HVL-VIA	2.6[b]	1.8[b]	0.1[b]	0	6.8[b]	7.4[b]	5.6[b]
(n = 10)	(2/4)	(1/3)	(0/0.6)	(0/0)	(4.4/9.1)	(5.8/8.3)	(4.8/6.6)
MEC	2.6[b]	2.1[b]	0.1[b]	0	7.1[b]	8.0[b]	5.8[b]
(n = 13)	(2/4)	(0.3/3)	(0/1.3)	(0/0)	(6.0/8.5)	(6.4/9.6)	(3.6/6.2)
P value*	<.001	<.001	.04		<.001	<.001	<.001

Abbreviations: PRRSV, porcine reproductive and respiratory syndrome virus; CON, control; UNIF, uninfected fetuses from inoculated dams; HVL-VIA, high viral load–viable fetuses; MEC, high viral load–meconium-stained fetuses. Fetuses used for VEGF and Ki67 labeling were similar but not identical. NA—viral load not assessed CON fetuses. PRRSV RNA concentration in copies per uL sera or mg tissue.
*Within each column, different superscripts indicate statistical group differences ($P < .05$) among fetal groups (Kruskal-Wallis with post hoc Dunn's test).

MEC (live fetus with >3.6 $\log_{10}$ genome copies per mg/μL in placenta, sera, and thymus and meconium staining of skin). All fetuses were spatially selected while considering their position in the uterine horns to obtain an equal distribution among and within litters (Supplemental Figures S1–S2).

Immunofluorescence

Assessment of angiogenesis in MFI tissues was determined through the detection of vascular endothelial growth factor (VEGF) using an anti-VEGFA rabbit polyclonal antibody (ab39250; 1:50 dilution; Abcam) and immunofluorescence. The antibody was raised against amino acids 1 to 100 of human VEGFA. Thus, to validate use of the antisera against VEGFA, a protein BLAST was conducted of *homo sapiens* (P15692.2) and *Sus scrofa* (P49151.1) VEGFA amino acid sequences. They were found to be 95% identical in the first 100 amino acids. Serially sectioned paraffin tissue blocks from CON (n = 9), UNIF (n = 9), HVL-VIA (n = 10), and MEC (n = 8) fetuses (Supplemental Figure S1) were labeled. While the objective was to include 10 fetuses per group, the distribution was not equal because the immunolabeling was of poor quality in some of the 3 samples of MFI within each paraffin block. To delineate cell borders and facilitate the identification of each cell type, sections were colabeled with tight junction protein-1 antibody (TJP-1; also known as zonula occludens-1; anti-ZO-1 rat monoclonal antibody IgG_{2a}; clone R40.76, sc-33725; 1:100 dilution; Santa Cruz Biotechnology), which identifies tight junctions to distinguish trophoblastic epithelium from uterine epithelium of the FMJ.[1] This antibody had been previously used in the pig to detect TJP-1.[14,16,28] A negative control was also labeled for each fetus by replacing the VEGF antibody with normal rabbit serum (ab7487; 1:10 dilution).

After deparaffinization and rehydration, 5-μm thick tissue sections on glass slides underwent antigen retrieval using Tris-EDTA (pH 9) for 30 minutes at 95°C. Primary antibodies were incubated on the slides overnight at 4°C. The respective secondary antibodies, donkey anti-rabbit-IgG (Cy[tm] 5, Jackson Immuno Research; 711545152; 1:200 dilution), and donkey anti-rat-IgG (Fluorescein [FITC], Jackson Immuno Research; 712095153; 1:200 dilution) were incubated for 4 h at room temperature. Counterstaining with 4′,6-diamidino-2-phenylindole (DAPI) was used to visualize cell nuclei. The slides were processed in 2 batches and nonspecific rabbit IgG was used at the same concentration as the primary antibody as a negative control.

Serial sections of paraffin tissues from the same fetuses, with 5 substitutions, that were used for VEGF labeling (Supplemental Figure S2), were immunolabeled for Ki-67 (anti-human Ki-67 mouse monoclonal; clone MIB-1 [Dako Omnis]; 1:100 dilution; Agilent Technologies), a proliferation marker expressed in the nuclei of proliferating cells.[40] This antibody has been previously used to evaluate porcine stem cell proliferation in jejunal crypts of intestinal samples.[8] Normal mouse serum (ab7486; 1:10 dilution) replaced the Ki-67 to demonstrate a lack of nonspecific binding for quality control purposes on the negative control slides. As described above, slides were also labeled for TJP-1 and DAPI. The secondary antibody used for the detection of Ki-67 was donkey anti-mouse-IgG (Rhodamine Red; Jackson Immuno Research; 711545152; 1:200 dilution). The same 4 fetal groups were assessed (n = 10 fetuses/group). The slides were processed in 2 batches and nonspecific mouse IgG was used with the same concentration as the primary antibody as a negative control. Immunolabeling details are outlined in Supplementary Tables S1 and S2.

Image Analysis

All sections and images were obtained and analyzed using an Olympus IX83 microscope system equipped with an Andor Zyla 4.2 sCMOS camera (2048 × 2048 pixel array; Andor USA, Concord, MA) and CellSens imaging software. In all

analyses, placental areolae and areas of detachment in the MFI were excluded. Evaluation and quantification of both placental angiogenesis and cell proliferation were performed with ImageJ using a series of semiautomated macros. For angiogenesis (detection of VEGF antibody), the ImageJ macro evaluated the median labeling intensity in each region (FMJ, submucosa, and myometrium). For this analysis, each region was analyzed in its entirety, and the median intensity values for each of the 3 samples (when suitable for analysis) were averaged to calculate a composite score for each region of each fetus.

For cell proliferation (detection of Ki-67 antibody), another ImageJ macro was developed to semiautomate the manual counting of positive cell nuclei per mm^2 of tissue independently in the uterine and trophoblast epithelium. For this analysis, representative sections of MFI were chosen by placing 3 identical rectangles (307,265 um^2) along the total length of the MFI of each of the 3 samples from each fetus. All measurements and imaging protocols were custom-developed for this study.

Statistical Analysis

All statistical analyses were performed using Stata 15.1 (StataCorp LP, TX, USA). Group differences in histological scores and PRRSV concentration were assessed using a Kruskal-Wallis with post hoc Dunn's test and Benjamin-Hochberg adjustment. The Ki67 and VEGF data were natural log-transformed to obtain a normal distribution. Differences in median VEGF pixel intensity (per mm^2) and counts of Ki67-positive labeled nuclei (per mm) among fetal classification groups were assessed using linear regression, followed by a pairwise comparison with Tukey multiple comparison adjustments. Full regression models were built that included other biologically relevant predictor variables (sex, within litter *Z*-score of brain: liver ratio [proxy for IUGR], and labeling batch) potentially associated with fetal PRRS severity, angiogenesis, and cell proliferation. A backward stepwise elimination was performed by removing nonsignificant variables until a parsimonious final model was achieved. For angiogenesis, separate models were created for each region investigated (FMJ, submucosa, and myometrium). For cell proliferation, separate models were created to assess labeling in the uterine and trophoblastic epithelium. For all analyses, $P < 0.05$ was considered statistically significant. All models were assessed for linearity and homoskedasticity of residuals using appropriate QQ and scatter plots.

Results

Histopathology and Viral Load

In the endometrial area of the MFI corresponding to infected fetuses, there was an accumulation of inflammatory cells (endometritis) characterized by lymphocytes, macrophages, and some plasma cells. An inflammatory reaction was also observed in the placental area (placentitis) associated with infected fetuses, with less severity than the endometrium, and characterized mainly by the accumulation of macrophages. In the endometrium associated with infected fetuses, there was accumulation of lymphocytes and occasional macrophages within vascular walls (vasculitis). Vasculitis was not observed in the placental area. In the CON fetuses, a few randomly distributed inflammatory cells were observed, without any vasculitis.

Among the samples from PRRSV-inoculated gilts, the severity of endometritis, placentitis, and endometrial vasculitis did not differ among the UNIF, HVL-VIA, and MEC groups. However, all PRRSV-inoculated groups had greater lesion scores ($P < .04$ for all) than the CON group, which had no inflammation in any of the 3 areas evaluated (Table 1).

Regarding PRRSV RNA concentration in the placenta, sera, and thymus, by experimental design, there were no statistical differences between the HVL-VIA and MEC fetal groups, but both groups had greater viral load than CON and UNIF fetuses ($P < .001$).

Localization of VEGF in the MFI

Immunolocalization of VEGF within the FMJ (Fig. 1) was more intense in the cytoplasm of trophoblastic epithelial cells compared with the cytoplasm of UEC (Fig. 2). In trophoblasts, the expression of VEGF appeared vesicular and with a tendency toward accumulation in the basolateral surface of the cell (Fig. 2). There was lower intensity of VEGF expression in UEC compared with trophoblasts, but it was possible to observe VEGF expression in the form of vesicles located mostly around the nucleus of UEC (Fig. 2).

In the endometrial submucosa, VEGF-positive immunolabeling was demonstrated in the cytoplasm of uterine glands (Fig. 3) with a spatial bias toward the apical part of the glandular cell (Fig. 4; suggesting the potential for diffuse release of VEGF into the glandular lumen). Also in endometrial submucosa, positive labeling for VEGF was detected through the entire cytoplasm of endothelial cells (Figs. 5, 6).

While the detection of VEGF was observed mainly in vesicular form in the cytoplasm of MFI cells mentioned above, the presence of positively immunolabeled vesicle-like structures were also detected in the extracellular spaces throughout the different regions evaluated. VEGF was also detected in myometrial cells (Fig. 7) in vesicle-like structures with random distribution in the cytoplasm (Fig. 8). These areas previously described as positive for VEGF labeling were identified in all fetuses evaluated without obvious visual difference between the groups.

Evaluation of VEGF Labeling Intensity by Fetal Group

Given the complex and diffuse labeling pattern described above, the analyses comparing differences in the intensity of VEGF labeling by fetal group were conducted on a whole-region basis (FMJ, uterine submucosa, and myometrium) rather

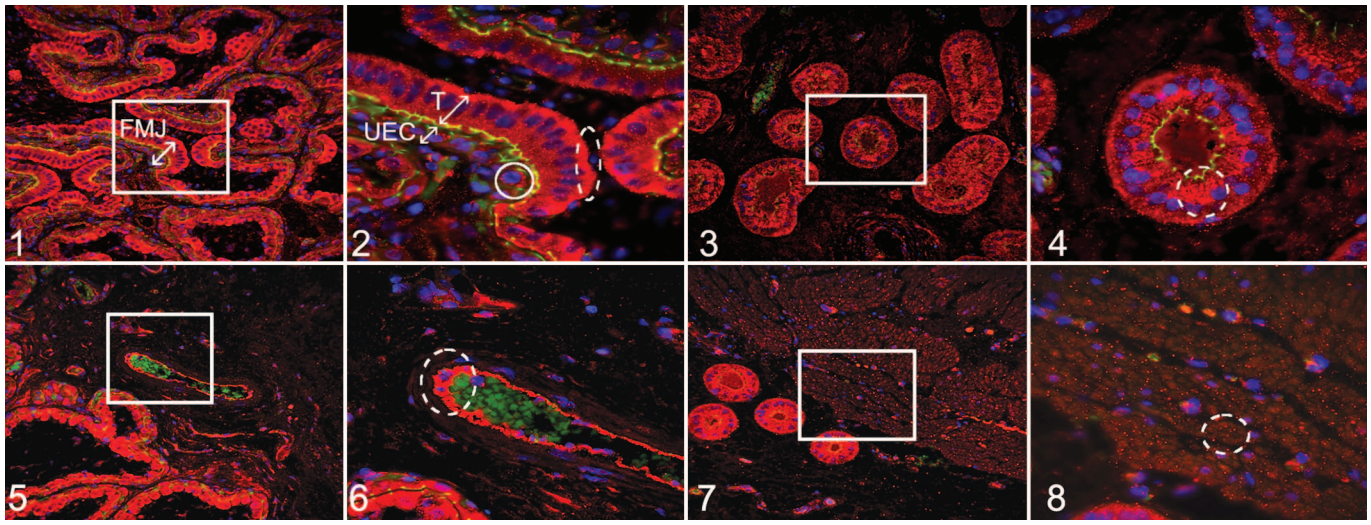

Figures 1–8. Porcine reproductive and respiratory syndrome virus 2 (PRRSV-2) at 12 days after maternal infection, uterus and placenta, pigs. Immunofluorescence for vascular endothelial growth factor (VEGF; red); 4′,6-diamidino-2-phenylindole (DAPI; blue; nuclear counterstaining); tight junction protein–1 (TJP-1; green; for identifying cell borders). **Figure 1.** Fetomaternal junction (FMJ) with diffusely positive immunolabeling for VEGF in all trophoblastic cells and with a higher intensity compared with uterine epithelial cells (UECs). **Figure 2.** Higher magnification of the white box in Figure 1. Trophoblasts (T) with diffuse VEGF expression in the cytoplasm and a tendency toward accumulation in the basolateral part of the cell (oval with dashed line). UECs have lower VEGF expression that is mostly observed around the nucleus (circle). **Figure 3.** Uterine glands have diffuse cytoplasmic labeling for VEGF. **Figure 4.** Higher magnification of the white box in Figure 3. There is diffuse VEGF immunolabeling with a tendency toward the apical part of the cell (oval with dashed line). **Figure 5.** Endothelial cells have diffuse cytoplasmic immunolabeling for VEGF. **Figure 6.** Higher magnification of the white box in Figure 5. There is diffuse immunolabeling through the cytoplasm (oval with dashed line). Autofluorescence of erythrocytes (green). **Figures 7**, **8.** Myometrial cells showing random foci of cytoplasmic immunolabeling for VEGF. Figure 8 is a higher magnification of the white box in Figure 7.

than by tissue type or element within region. The resulting analysis (Figs. 9–11) showed that group differences were only significant ($P = .05$) in the submucosa, with greater expression of VEGF observed in endometrium associated with UNIF and HVL-VIA fetuses compared with MEC, with CON being intermediary (Fig. 10). Regarding the potential effects of sex and IUGR on VEGF labeling intensity, a significant association was only demonstrated in the submucosa where intensity was greater for female versus male ($P = .027$) fetuses, and inversely related to brain: liver weight ratio (lower intensity in IUGR vs non-IUGR fetuses; $P = .013$; Fig. 12). Labeling batch was also significantly associated with intensity in the submucosa ($P = .003$) and myometrial ($P = .02$) regions, but not in FMJ.

Localization of Ki-67 in the MFI

Immunolocalization of Ki-67 was randomly detected throughout the MFI in both trophoblastic epithelium and UEC (Fig. 13) and as expected was exclusively found in the nucleus (Fig. 14). Ki-67 protein was granular to condensed and observed scattered throughout the nuclei.

Evaluation of Positive Ki-67 Labeling by Fetal Group

In the maternal epithelium, the number of Ki-67 labeled cells differed across fetal classification groups ($P < .001$) with CON and UNIF groups having greater Ki-67 counts (indicative of greater proliferation) in UEC compared with the VIA and MEC groups (Fig. 15). Significant group differences were also observed among the fetal disease progression groups with respect to the number of Ki-67 positive trophoblastic epithelial cells ($P = .001$). Greater trophoblastic cell proliferation was evident in the CON group compared with all infected groups (Fig. 16).

Neither sex nor brain: liver ratio was associated with Ki67 labeling in the maternal and fetal epithelium. However, labeling batch was significant ($P < .001$) for both types of cells, with greater labeling intensity in the second versus the first batch.

Discussion

The objective of this study was to evaluate angiogenesis and cell proliferation in the porcine MFI to determine if these processes were altered by PRRSV-2 infection. Examining VEGF immunofluorescence labeling intensity and count of nuclei immunopositive for Ki67 in MFI tissues across fetal phenotypic groups representing a range of disease progression from noninfected to high viral load–MEC, provided insight into the possible mechanisms of fetal compromise.

With regard to reproductive PRRS, it has been shown that the infection of uterine tissues and transplacental transmission of PRRSV-2 to the fetus occurs rapidly. After intramuscular/intranasal viral inoculation in the gilts, viral replication in uterine

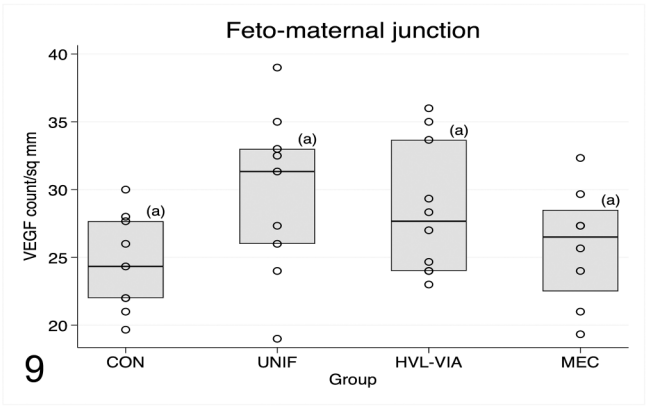

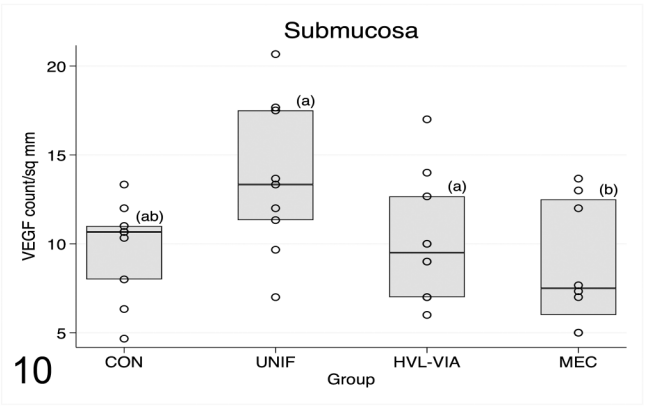

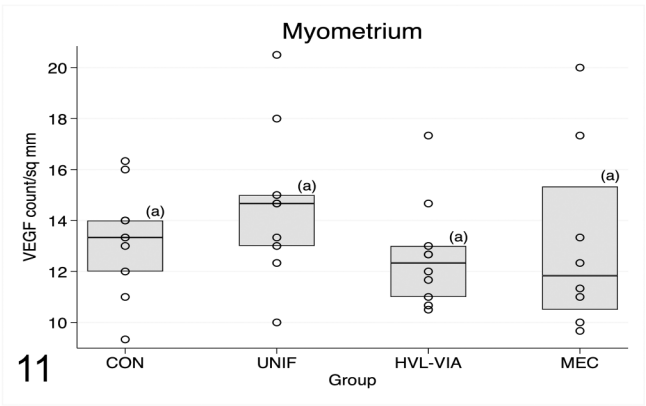

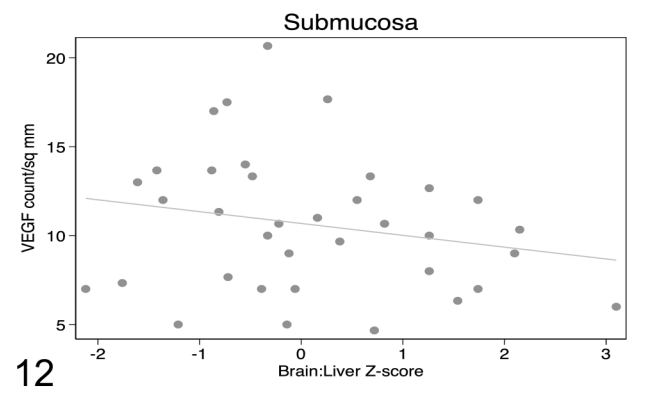

Figures 9–12. Box plots comparing vascular endothelial growth factor (VEGF) immunolabeling counts per mm^2 among fetal porcine reproductive and respiratory syndrome virus 2 (PRRSV-2) resilience groups: control (CON), uninfected (UNIF), high viral load–viable (HVL-VIA), and meconium-stained (MEC). Each datapoint represents the average of 3 different regions of the maternal-fetal interface (MFI), for each fetus. Different superscripts indicate significant group differences based on Tukey-adjusted post hoc pairwise comparisons from linear regression modeling of ln-transformed data. **Figure 9.** Fetomaternal junction. No significant differences are observed ($P = .08$). **Figure 10.** Submucosa. VEGF immunolabeling intensity is significantly lower in MEC versus UNIF and HVL-VIA groups ($P = .0001$). **Figure 11.** Myometrium. No significant differences among groups are observed ($P = .09$). **Figure 12.** Submucosa, showing the relationship between VEGF labeling and brain: liver weight ratio, a proxy measure for intrauterine growth restriction. Fetuses with intrauterine growth restriction (IUGR; those with greater brain: liver ratios) have lower VEGF labeling ($P = .013$).

tissues occurs within 2 days and transplacental transmission of the virus to fetuses is evident within 5 days.[26] The virus has been demonstrated in different fetal organs including thymus, tonsils, lymph nodes, lungs, liver, spleen, heart, and kidneys following infection.[26,27,38] Classification of fetuses along a spectrum of relative fetal resilience based on fetal preservation and viral load is highly desirable to study PRRSV-2 pathogenesis. UNIF fetuses are classified as more resistant to the virus than the HVL groups because viral replication is suppressed or prevented in fetal tissues. The UNIF fetuses were purposely selected for this study based on absence of virus in placenta, sera, and fetal thymus. By contrast, HVL-VIA and MEC fetuses had high levels of virus in all 3 tissues tested. Previous research has proposed that viable fetuses with HVLs are more tolerant than their MEC cohorts that show early to advanced signs of fetal compromise preceding death.[22,26,33,47] The relationship between viral infection and fetal death has been difficult to understand in part because microscopic lesions are limited in the fetus in both research and diagnostic specimens.[9,23,32,37] On the other hand, another fundamental organ during pig pregnancy that has been widely evaluated during PRRSV infections is the placenta. Frequent inflammatory lesions associated with PRRSV infection are observed in the endometrium, placenta, myometrium, and blood vessels, along with hemorrhagic areas, apoptotic cell death in MFI cells, and areas of separation between trophoblasts and UEC.[18,19,30,31] These PRRSV-related lesions in the MFI have historically been considered important in terms of the possible mechanisms of fetal death.

Angiogenesis is a process involving the formation and development of new blood vessels from the existing vasculature[12] and is an essential physiological component of placental development during pregnancy to enhance the exchange of gases and nutrients between the dam and litter.[5] While contributing to placental development,[3] the importance of angiogenesis in placental tissues during pregnancy is highlighted best by the alterations in angiogenesis that can compromise pregnancies in animals

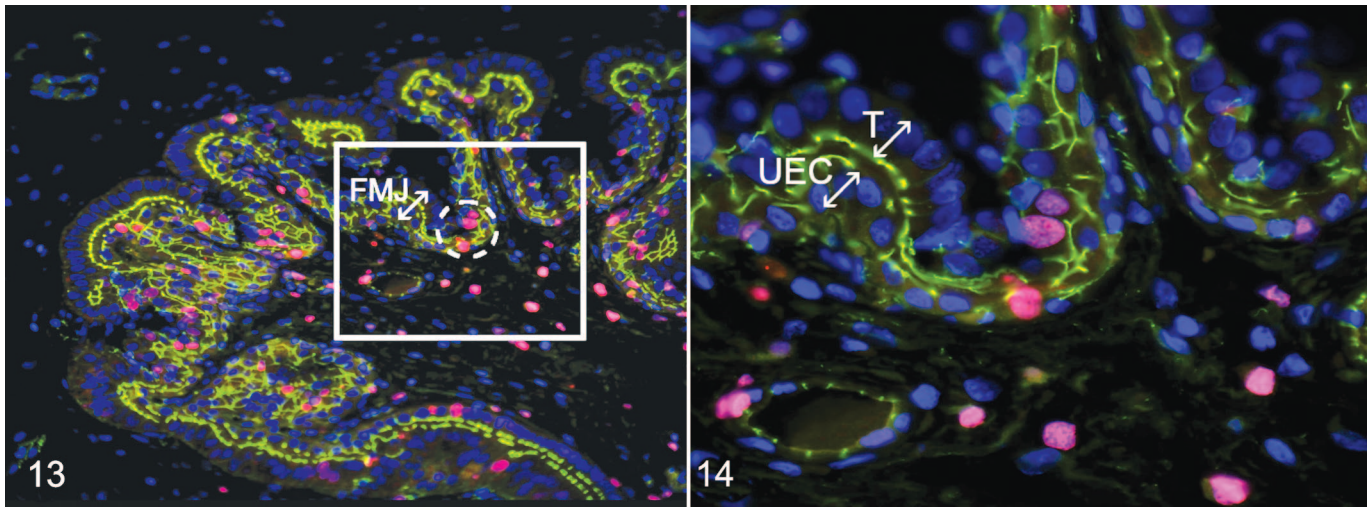

Figures 13, 14. Porcine reproductive and respiratory syndrome virus 2 (PRRSV-2) at 12 days after maternal infection, fetomaternal junction (FMJ), pigs. Immunofluorescence for Ki67 (pink); 4′,6-diamidino-2-phenylindole (DAPI; blue; nuclear counterstaining); tight junction protein-1 (TJP-1; green; for identifying cell borders). **Figure 13.** Trophoblast and uterine epithelial cells (UECs) showing positive labeling for Ki67 expressed randomly throughout the FMJ (ovals with dashed line). **Figure 14.** Higher magnification of the white box in Figure 13. There is positive labeling for Ki67 in the nucleus of trophoblastic (T) cells and nucleus of UECs.

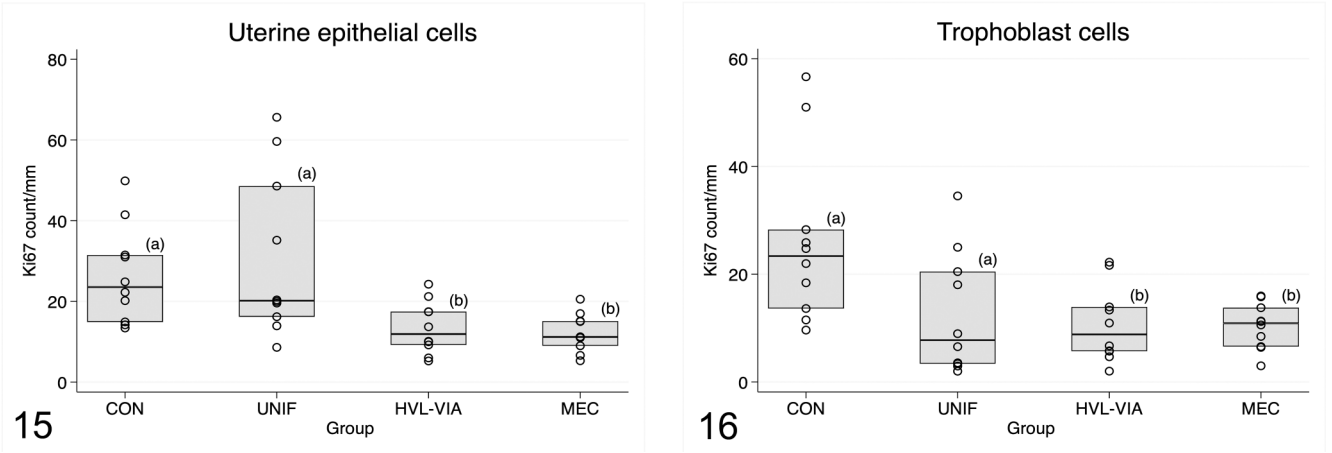

Figures 15, 16. Box plots comparing Ki67 immunolabeling counts per mm among fetal porcine reproductive and respiratory syndrome virus 2 (PRRSV-2) resilience groups: control (CON), uninfected (UNIF), high viral load–viable (HVL-VIA), and meconium-stained (MEC). Each datapoint represents values for epithelial layers of the fetomaternal junction associated with each individual fetus. Different superscripts indicate significant group differences based on Tukey-adjusted post hoc pairwise comparisons from linear regression modeling of ln-transformed data. **Figure 15.** Uterine epithelial cells. There is significantly decreased Ki-67 immunolabeling (lower cell proliferation) in HVL-VIA and MEC groups ($P < .001$). **Figure 16.** Trophoblast cells. There is significantly decreased Ki-67 immunolabeling in all fetal groups from infected gilts compared with non-inoculated control gilts ($P = .001$).

and women.[10,20,35,36] VEGF is one of several angiogenic factors that participate in the formation and development of new blood vessels in the placenta[4,11] through its involvement in stimulating mitosis and proliferation of endothelial cells. While intuitive that VEGF immmunolabeling should be localized around endothelial cells, in the present study, VEGF immunolabeling was also localized in uterine and trophoblastic epithelium, uterine gland cells, and myometrial cells. These results are consistent with previous investigations where VEGF was detected in different types of porcine placental cells.[6,15,48,49] It has been proposed that extra-endothelial localization of VEGF in cells, such as the uterine or trophoblastic epithelium, might be related to the differentiation and cell maturation functions that VEGF produces in these cells.[49,50] Similarly, the expression of VEGF in the uterine glandular epithelium might be associated with the differentiation, development, and secretory functions that VEGF promotes in the glandular cells.[49]

Despite the similarity in the area of MFI among the fetal groups in our study, MEC fetuses presented a lower expression of VEGF in the endometrial submucosa where abundant

uterine glands and blood vessels are located. Considering the numerous functions that VEGF has on these cellular structures, low expression of VEGF in the submucosa associated with MEC fetuses may negatively affect cellular transport capacities in placental cells, mitosis, development, and differentiation of uterine glands and endothelial cells compromising normal fetal development and survival of these fetuses, thereby resulting in fetal compromise and meconium staining following PRRSV infection. Another possible reason for the decreased expression of VEGF in MEC fetuses may be related to the other pathological processes induced by PRRSV.

The VEGF immunolabeling in the cytoplasm of MFI cells and in extracellular areas suggests that the cellular storage and release of this glycoprotein to the extracellular medium may be carried via vesicles. This vesicular form could lead to signaling between cells and the resulting angiogenic effects of VEGF between neighboring or distant cells.[13,45]

In the present study, female fetuses presented with significantly greater levels of VEGF immunolabeling in the submucosa associated with male fetuses and trended similarly in the MFI. Finding sex differences was not entirely unexpected as these were reported for angiogenic signaling in tissue of the porcine MFI.[41] Although these previous differences were detected in vitro, it suggests that male and female fetuses communicate differently during different periods of gestation (preimplantation, migrating around the uterus, and implantation). Based on the present results, it is also plausible that male and female fetuses might have differing angiogenic responses when infected by PRRSV.

The angiogenic response in IUGR fetuses in this study are partially consistent with other investigations that suggest that VEGF may be an important growth factor associated with fetal development, and alterations in placental angiogenesis may predispose to compromised nutrient transport due to alterations in the development of new placental blood vessels[15,36] While the reduction in VEGF immunolabeling in IUGR fetuses in this study was only noted in the submucosa and its effect was variable, IUGR fetuses that have lower viral loads are at greater odds of being UNIF compared with non-IUGR littermates.[21] It is possible that the lower vascularization in IUGR fetuses could reduce the opportunity for transplacental infection because of fewer vessels or increase the distance separating maternal and fetal circulation at the FMJ.

Ki-67 was used to evaluate cell proliferation because the protein is expressed in the nucleus of cells in a state of proliferation, and its immunoreactivity is detected at all stages of the cell cycle except G_0 or resting phase.[40] In this study, Ki-67 was detected in both endometrial cells and trophoblastic epithelium indicating proliferation of these cell types during pregnancy. The labeling differentiated cells in a state of proliferation (pink label—Ki-67) and quiescent cells (blue labeling—DAPI) along the FMJ.

In the UEC, Ki-67 immunoreactivity was statistically different among fetal classification groups, with CON and UNIF fetuses having greater cell proliferation than the infected HVL-VIA and MEC groups. This suggests that proliferation of uterine epithelium is reduced following PRRSV infection, but only after the fetus is infected. This is noteworthy because the severity of endometritis and vasculitis in UNIF fetuses was similar to the other infected groups (Table 1) suggesting endometrial disease is not underlying proliferation of UEC. By contrast, Ki-67 immunoreactivity in trophoblastic epithelial cells was decreased in all fetal groups from inoculated gilts (UNIF, VIA, and MEC) compared with CON fetuses. This suggests the continuous remodeling of trophoblast cells that normally occurs during porcine gestation is adversely affected as soon as the endometrium is PRRSV-infected, independent of fetal infection. This may be due to apoptotic cell death in placental cells of the MFI.[19,31] Arrested cell cycle was confirmed during PRRSV-2 infection of cultured porcine trophoblast cells at the G2/M phase.[42]

These results also support the concept of cross-talk between the fetus and MFI whereby some host responses in MFI are only induced after fetal infection is established. For example, a core set of interferon-induced genes were upregulated in fetal placenta and thymus of LVL and HVL fetuses, but only after the fetal thymus became infected.[47] These genes were not upregulated in UNIF fetuses, or in fetuses with infected placenta but UNIF thymus.[47] Our results indicate that the cell cycle is downregulated in trophoblasts prior to fetal infection and in the opposing uterine epithelium after fetal infection.

It was previously demonstrated that the decrease in cell proliferation factors in placental tissues was associated with the lightest fetuses and IUGR during different periods of gestation, potentially affecting cell proliferation or remodeling and the exchange of nutrients between the dam and the fetus during development.[7,41] While our results demonstrate that VEGF labeling was decreased in the submucosa associated with IUGR fetuses, no such relationship was found to be associated with the amount of Ki67 immunoreactivity.

Conclusion

Angiogenesis and proliferation of maternal and placental cells are indispensable physiological processes during pregnancy that ensure adequate development and maintenance of MFI tissues while also ensuring the proper development and survival of the fetus. PRRSV has direct and indirect effects on different types of reproductive tissues through inflammatory processes, apoptosis, and cell cycle arrest. Fetuses classified as resistant to PRRSV infection due to lack of virus detected in fetal tissues (UNIF) demonstrated levels of angiogenesis in the submucosa and cell proliferation in UEC similar to those of CON fetuses. Thus, the homeostasis of angiogenesis in the endometrium of UNIF fetuses could be described as a characteristic of resistance to PRRSV infection. By contrast, decreased angiogenesis was observed in the submucosa of the most susceptible fetuses (MEC) and may underlie an important mechanism associated with fetal demise. Furthermore, decreased angiogenesis in the submucosa of IUGR fetuses may help to prevent PRRSV infection, explaining the relative resilience of this phenotype. While trophoblast cell proliferation decreased in all fetuses postinfection, similar changes in the UEC appear to be dependent on

infection of the fetus. None of these changes, however, were related to severity of endometritis, placentitis, or endometrial vasculitis. In addition to the pathological effects that PRRSV produced in endometrial and placental tissues reported in other investigations, we confirm that PRRSV infection of reproductive tissues also decreases VEGF immunolabeling intensity which plausibly alters angiogenesis in the submucosa and cell proliferation in MFI cells and thereby adversely affects fetal viability.

Acknowledgments

The authors acknowledge the Prairie Diagnostic Services Inc. and many technicians and students who assisted with the animal experiment. Special thanks to Larhonda Sobchishin and Eiko Kawamura for their assistance with the microscopy work and to the PGM team members who provided positive suggestions.

Author Contributions

All authors participated in experiment design and sample collection. Staining and microscopy was performed by JAB-Z with technical assistance from DJM, JAP, and GH. Statistical analysis was completed by JAB-Z and JCSH. Pathological oversight was provided by SED. JAB-Z, SED, and JCSH drafted the manuscript. All authors contributed to and approved the final version.

Declaration of Conflicting Interests

The author(s) declared no potential conflicts of interest with respect to the research, authorship, and/or publication of this article.

Funding

The author(s) disclosed receipt of the following financial support for the research, authorship, and/or publication of this article: Funding was generously provided by Genome Canada (Project 2014LSARP_8202) and Genome Prairie (Saskatchewan Ministry of Agriculture, Project #346143) with administrative support provided by Genome Alberta.

ORCID iD

Susan E. Detmer https://orcid.org/0000-0002-4064-3460

References

1. Anderson JM, Stevenson BR, Jesaitis LA, et al. Characterization of ZO-1, a protein component of the tight junction from mouse liver and Madin-Darby canine kidney cells. *J Cell Biol*. 1988;**106**:1141–1149.
2. Bauer R, Walter B, Hoppe A, et al. Body weight distribution and organ size in newborn swine (sus scrofa domestica)—a study describing an animal model for asymmetrical intrauterine growth retardation. *Exp Toxicol Pathol*. 1998;**50**:59–65.
3. Burton G, Charnock-Jones D, Jauniaux E. Regulation of vascular growth and function in the human placenta. *Reproduction*. 2009;**138**:895–902.
4. Carmeliet P. Mechanisms of angiogenesis and arteriogenesis. *Nat Med*. 2000;**6**:389–395.
5. Carter AM. Evolution of placental function in mammals: the molecular basis of gas and nutrient transfer, hormone secretion, and immune responses. *Physiol Rev*. 2012;**92**:1543–1576.
6. Charnock-Jones DS, Clark DE, Licence D, et al. Distribution of vascular endothelial growth factor (VEGF) and its binding sites at the maternal-fetal interface during gestation in pigs. *Reproduction*. 2001;**122**:753–760.
7. Chen F, Wang T, Feng C, et al. Proteome differences in placenta and endometrium between normal and intrauterine growth restricted pig fetuses. *PLoS ONE*. 2015;**10**:e0142396.
8. Chen Y-M, Helm ET, Groeltz-Thrush JM, et al. Epithelial-mesenchymal transition of absorptive enterocytes and depletion of Peyer's patch M cells after PEDV infection. *Virology*. 2021;**552**:43–51.
9. Cheon D-S, Chae C. Distribution of porcine reproductive and respiratory syndrome virus in stillborn and liveborn piglets from experimentally infected sows. *J Comp Pathol*. 2001;**124**:231–237.
10. Conroy A, Serghides L, Finney C, et al. C5a enhances dysregulated inflammatory and angiogenic responses to malaria in vitro: potential implications for placental malaria. *PLoS ONE*. 2009;**4**:e4953.
11. Ferrara N. Role of vascular endothelial growth factor in regulation of physiological angiogenesis. *Am J Physiol cell Physiol*. 2001;**280**:C1358–C1366.
12. Folkman J. Angiogenesis. *Biol Endo Cells*. 1984;**27**:412–428.
13. Gai C, Carpanetto A, Deregibus MC, Camussi G. Extracellular vesicle-mediated modulation of angiogenesis. *Histol Histop*. 2016;**31**:379–391.
14. Guidoni PB, Pasternak JA, Hamonic G, et al. Decreased tight junction protein intensity in the placenta of porcine reproductive and respiratory syndrome virus-2 infected fetuses. *Placenta*. 2021;**112**:153–161.
15. Guimarães GC, Alves LA, Betarelli RP, et al. Expression of vascular endothelial growth factor (VEGF) and factor VIII in the gilt placenta and its relation to fetal development. *Theriogenology*. 2017;**92**:63–68.
16. Hamonic G, Pasternak JA, Forsberg NM, et al. Expression of pattern recognition receptors in porcine uterine epithelial cells in vivo and in culture. *Vet Immunol Immunopathol*. 2018;**202**:1–10.
17. Holtkamp DJ, Kliebenstein JB, Neumann EJ, et al. Assessment of the economic impact of porcine reproductive and respiratory syndrome virus on United States pork producers. *J Swine Heal Prod*. 2013;**21**:72–84.
18. Karniychuk UU, Nauwynck HJ. Pathogenesis and prevention of placental and transplacental porcine reproductive and respiratory syndrome virus infection. *Veter Res*. 2013;**44**:1–14.
19. Karniychuk UU, Saha D, Geldhof M, et al. Porcine reproductive and respiratory syndrome virus (PRRSV) causes apoptosis during its replication in fetal implantation sites. *Microb Path*. 2011;**51**:194–202.
20. Lacko LA, Hurtado R, Hinds S, et al. Altered feto-placental vascularization, feto-placental malperfusion and fetal growth restriction in mice with Egfl7 loss of function. *Development*. 2017;**144**:2469–2479.
21. Ladinig A, Foxcroft G, Ashley C, et al. Birth weight, intrauterine growth retardation and fetal susceptibility to porcine reproductive and respiratory syndrome virus. *PLoS ONE*. 2014;**9**:e109541.
22. Ladinig A, Wilkinson J, Ashley C, et al. Variation in fetal outcome, viral load and ORF5 sequence mutations in a large scale study of phenotypic responses to late gestation exposure to type 2 porcine reproductive and respiratory syndrome virus. *PLoS ONE*. 2014;**9**:e96104.
23. Lager KM, Halbur PG. Gross and microscopic lesions in porcine fetuses infected with porcine reproductive and respiratory syndrome virus. *J Vet Diagn Invest*. 1996;**8**:275–282.
24. Loving CL, Osorio FA, Murtaugh MP, Zuckermann FA. Innate and adaptive immunity against porcine reproductive and respiratory syndrome virus. *Vet Immunol Immuno*. 2015;**167**:1–14.
25. Malgarin CM, Moser F, Pasternak JA, et al. Fetal hypoxia and apoptosis following maternal porcine reproductive and respiratory syndrome virus (PRRSV) infection. *BMC Vet Res*. 2021;**17**:1–14.
26. Malgarin CM, Nosach R, Novakovic P, et al. Classification of fetal resilience to porcine reproductive and respiratory syndrome (PRRS) based on temporal viral load in late gestation maternal tissues and fetuses. *Virus Res*. 2019;**260**:151–162.
27. Mengeling WL, Lager K, Vorwald A. Temporal characterization of transplacental infection of porcine fetuses with porcine reproductive and respiratory syndrome virus. *Am J Vet Res*. 1994;**55**:1391–1398.
28. Miller AL, Pasternak JA, Medeiros NJ, et al. In vivo synthesis of bacterial amyloid curli contributes to joint inflammation during S. Typhimurium Infection. *PLoS Pathog*. 2020;**16**:e1008591.

29. Moura CAA, Johnson C, Baker SR, et al. Assessment of immediate production impact following attenuated PRRS type 2 virus vaccination in swine breeding herds. *Porcine Heal Manage*. 2019;**5**:13.
30. Novakovic P, Detmer SE, Suleman M, et al. Histologic changes associated with placental separation in gilts infected with porcine reproductive and respiratory syndrome virus. *Vet Pathol*. 2018;**55**:521–530.
31. Novakovic P, Harding JC, Al-Dissi AN, Detmer SE. Type 2 porcine reproductive and respiratory syndrome virus infection increases apoptosis at the maternal-fetal interface in late gestation pregnant gilts. *PLoS ONE*. 2017;**12**:e0173360.
32. Novakovic P, Harding JC, Al-Dissi AN, et al. Pathologic evaluation of type 2 porcine reproductive and respiratory syndrome virus infection at the maternal-fetal interface of late gestation pregnant gilts. *PLoS ONE*. 2016;**11**:e0151198.
33. Pasternak JA, MacPhee DJ, Harding JC. Fetal cytokine response to porcine reproductive and respiratory syndrome virus-2 infection. *Cytokine*. 2020;**126**:154883.
34. Pasternak JA, MacPhee DJ, Harding JC. Maternal and fetal thyroid dysfunction following porcine reproductive and respiratory syndrome virus2 infection. *Vet Res*. 2020;**51**:1–14.
35. Redman CW, Sargent IL. Latest advances in understanding preeclampsia. *Science*. 2005;**308**:1592–1594.
36. Reynolds LP, Caton JS, Redmer DA, et al. Evidence for altered placental blood flow and vascularity in compromised pregnancies. *J Physiol*. 2006;**572**:51–58.
37. Rossow K, Laube K, Goyal S, Collins J. Fetal microscopic lesions in porcine reproductive and respiratory syndrome virus-induced abortion. *Veter Pathol*. 1996;**33**:95–99.
38. Rowland RR. The interaction between PRRSV and the late gestation pig fetus. *Virus Res*. 2010;**154**:114–122.
39. Sanchis EG, Cristofolini AL, Fiorimanti MR, et al. Apoptosis and cell proliferation in porcine placental vascularization. *Animal Reprod Sci*. 2017;**184**:20–28.
40. Scholzen T, Gerdes J. The Ki-67 protein: from the known and the unknown. *J Cell Physiol*. 2000;**182**:311–322.
41. Stenhouse C, Hogg CO, Ashworth CJ. Associations between fetal size, sex and both proliferation and apoptosis at the porcine feto-maternal interface. *Placenta*. 2018;**70**:15–24.
42. Suleman M, Novakovic P, Malgarin C, et al. Spatiotemporal immunofluorescent evaluation of porcine reproductive and respiratory syndrome virus transmission across the maternal-fetal interface. *Path Dis*. 2018;**76**:fty060.
43. Terpstra C, Wensvoort G, Pol J. Experimental reproduction of porcine epidemic abortion and respiratory syndrome (mystery swine disease) by infection with Lelystad vims: Koch's postulates fulfilled. *Veter Quart*. 1991;**13**:131–136.
44. Thomann B, Rushton J, Schuepbach-Regula G, Nathues H. Modeling economic effects of vaccination against porcine reproductive and respiratory syndrome: impact of vaccination effectiveness, vaccine price, and vaccination coverage. *Front Vet Sci*. 2020;**7**:500.
45. Todorova D, Simoncini S, Lacroix R, et al. Extracellular vesicles in angiogenesis. *Circ Res*. 2017;**120**:1658–1673.
46. Vallet J, Freking B. Differences in placental structure during gestation associated with large and small pig fetuses. *J Anim Sci*. 2007;**85**:3267–3275.
47. Van Goor A, Pasternak A, Walker K, et al. Differential responses in placenta and fetal thymus at 12 days post infection elucidate mechanisms of viral level and fetal compromise following PRRSV2 infection. *BMC Genomics*. 2020;**21**:1–20.
48. Vonnahme KA, Ford SP. Placental vascular endothelial growth factor receptor system mRNA expression in pigs selected for placental efficiency. *J Physiol*. 2004;**554**:194–201.
49. Winther H, Ahmed A, Dantzer V. Immunohistochemical localization of vascular endothelial growth factor (VEGF) and its two specific receptors, Flt-1 and KDR, in the porcine placenta and non-pregnant uterus. *Placenta*. 1999;**20**:35–43.
50. Zhou Y, McMaster M, Woo K, et al. Vascular endothelial growth factor ligands and receptors that regulate human cytotrophoblast survival are dysregulated in severe preeclampsia and hemolysis, elevated liver enzymes, and low platelets syndrome. *Am J Pathol*. 2002;**160**:1405–1423.